Magnetic effects in heavy-ion collisions at intermediate energies

Li Ou[1,2,*] and Bao-An Li[1,†]

[1]*Department of Physics and Astronomy, Texas A&M University-Commerce, Commerce, Texas 75429-3011, USA*

[2]*College of Physics and Technology, Guangxi Normal University, Guilin 541004, People's Republic of China*

(Received 14 July 2011; revised manuscript received 12 October 2011; published 14 December 2011)

The time evolution and space distribution of internal electromagnetic fields in heavy-ion reactions at beam energies between 200 and 2000 MeV/nucleon are studied within an isospin-dependent Boltzmann-Uhling-Uhlenbeck transport model (IBUU11). While the magnetic field can reach about 7×10^{16} G, which is significantly higher than the estimated surface magnetic field ($\sim 1 \times 10^{15}$ G) of magnetars, it has almost no effect on nucleon observables because the Lorentz force is normally much weaker than the nuclear force. Very interestingly, however, the magnetic field generated by the projectilelike (targetlike) spectator has a strong focusing and defocusing effect on positive and negative pions at forward (backward) rapidities. Consequently, the differential π^-/π^+ ratio as a function of rapidity is significantly altered by the magnetic field, whereas the total multiplicities of both positive and negative pions remain about the same. At beam energies above about 1 GeV/nucleon, while the integrated ratio of total π^- to π^+ multiplicities is not, the differential π^-/π^+ ratio is sensitive to the density dependence of nuclear symmetry energy $E_{\rm sym}(\rho)$. Our findings suggest that magnetic effects should be carefully considered in future studies of using the differential π^-/π^+ ratio as a probe of the $E_{\rm sym}(\rho)$ at suprasaturation densities.

DOI: 10.1103/PhysRevC.84.064605 PACS number(s): 25.70.−z, 21.65.Ef, 24.10.Nz, 41.20.−q

I. INTRODUCTION

Magnetic fields exist everywhere in the universe. To set the scale and appreciate the strong magnetic fields created during heavy-ion collisions, we first recall the magnitudes of several typical magnetic fields from various sources. Many spiral galaxies have magnetic fields with a typical strength of $\sim 3 \times 10^{-6}$ G [1] and it is estimated that the intergalactic magnetic fields presently have an intensity of about $\leqslant 1 \times 10^{-9}$ G [2]. Some people believe that the present magnetic field of the universe was amplified from a seed of about 1×10^{-20} G by the dynamo mechanism [3,4], whereas magnetic fields up to 1×10^{24} G might appear in the early universe [4]. The strongest magnetic field of about 1×10^{15} G near the surfaces of magnetars [5,6] or even higher (1×10^{16} to 1×10^{17} G) associated with the cosmological γ-ray bursts [7] have been found from astrophysical observations. Owing to the limit of the tensile strength of terrestrial materials, the strongest man-made steady magnetic field is only about 4.5×10^5 G [8,9]. To our best knowledge, it was first pointed out by Rafelski and Müller that, in addition to strong electrical fields, unusually strong magnetic fields are also created in heavy-ion collisions (HICs). In sub-Coulomb barrier U + U collisions, the magnetic field was estimated to be on the order of 1×10^{14} G [10]. More recently, it was shown by Kharzeev *et al.* that HICs at the Relativistic Heavy Ion Collider (RHIC) and the Large Hadron Collider can create the strongest magnetic field ever achieved in a terrestrial laboratory [11]. For example, in noncentral Au + Au collisions at 100 GeV/nucleon, the maximal magnetic field can reach about 1×10^{17} G [11,12]. It thus provides a unique environment to investigate QCD at the limit of high magnetic field. Indeed, the study of quark-gluon plasma under strong magnetic field has attracted much attention in the high-energy heavy-ion community (see, e.g., Ref. [13] and references therein). In particular, it was shown theoretically that [11,14–16] QCD topological effects in the presence of very intense electromagnetic fields (i.e., the "chiral magnetic effect") may be evidence of local parity violation in strong interactions. Experimentally, interesting indications have been reported (see, e.g., Refs. [17,18]).

Stimulated by the interesting findings at RHIC and realizing that all transport model studies of magnetic effects have so far focused on high-energy HICs [12,19], we investigate in this work first the strength, duration, and distribution of internal magnetic fields created in HICs at beam energies between 200 and 2000 MeV/nucleon. This is the beam-energy range covered by several accelerators in the world. We then focus on identifying possible magnetic effects on experimental observables using an isospin-dependent Boltzmann-Uhling-Uhlenbeck (BUU) transport model, IBUU11 [20,21]. We find that while the magnetic field can reach about 7×10^{16} G in these reactions, it has almost no effect on nucleon observables because the Lorentz force is negligibly small compared to the nuclear force. Very interestingly, however, the magnetic field generated by the projectilelike (targetlike) spectator moving forward (backward) in the center-of-mass frame has a strong focusing and defocusing effect on positive and negative pions moving forward (backward). As a result, the differential π^-/π^+ ratio as a function of rapidity is significantly altered by the magnetic field, whereas the total π^- and π^+ multiplicities remain about the same.

The paper is organized as follows. In the next section, we outline how the internal electromagnetic fields in HICs are calculated in the IBUU11 transport model. The characteristics of the electromagnetic fields and their effects on several experimental observables in intermediate-energy HICs are

*only.ouli@gmail.com

†bao-an_li@tamu-commerce.edu

then discussed in Sec. III. Finally, a summary is given at the end.

II. THE MODEL

In the presence of electrical and magnetic fields $\boldsymbol{E}$ and $\boldsymbol{B}$, the BUU equation can be written as

$$\left[\frac{\partial}{\partial t}+\frac{\boldsymbol{P}}{E}\nabla_r-(\nabla_r U-q\boldsymbol{v}\times\boldsymbol{B}-q\boldsymbol{E})\nabla_p\right]f(\boldsymbol{r},\boldsymbol{p},t)=I(\boldsymbol{r},\boldsymbol{p},t), \quad (1)$$

where $I(\boldsymbol{r},\boldsymbol{p},t)$ is the collision integral simulated by using the Monte Carlo method. The electrical field $\boldsymbol{E}$ (Coulomb field) has already been considered in most transport models. To include consistently both electrical and magnetic fields satisfying Maxwell's equations, the Liénard-Wiechert potentials at a position $\boldsymbol{r}$ and time t are evaluated according to

$$e\boldsymbol{E}(\boldsymbol{r},t)=\frac{e^2}{4\pi\epsilon_0}\sum_n Z_n\frac{c^2-v_n^2}{(cR_n-\boldsymbol{R}_n\cdot\boldsymbol{v}_n)^3}(c\boldsymbol{R}_n-R_n\boldsymbol{v}_n) \quad (2)$$

and

$$e\boldsymbol{B}(\boldsymbol{r},t)=\frac{e^2}{4\pi\epsilon_0 c}\sum_n Z_n\frac{c^2-v_n^2}{(cR_n-\boldsymbol{R}_n\cdot\boldsymbol{v}_n)^3}\boldsymbol{v}_n\times\boldsymbol{R}_n, \quad (3)$$

where Z_n is the charge number of the nth particle; $\boldsymbol{R}_n=\boldsymbol{r}-\boldsymbol{r}'_n$ is the relative position of the field point $\boldsymbol{r}$ with respect to the position $\boldsymbol{r}'_n$ of particle n moving with velocity $\boldsymbol{v}_n$ at the retarded time $t_{rn}=t-|\boldsymbol{r}-\boldsymbol{r}'_n(t_{rn})|/c$. The summation runs over all charged particles in the reaction system. In nonrelativistic cases (i.e., when all particles satisfy the condition $v\ll c$), Eqs. (2) and (3) reduce to the familiar expressions

$$e\boldsymbol{E}(\boldsymbol{r},t)=\frac{e^2}{4\pi\epsilon_0}\sum_n Z_n\frac{1}{R_n^3}\boldsymbol{R}_n \quad (4)$$

and

$$e\boldsymbol{B}(\boldsymbol{r},t)=\frac{e^2}{4\pi\epsilon_0 c^2}\sum_n Z_n\frac{1}{R_n^3}\boldsymbol{v}_n\times\boldsymbol{R}_n. \quad (5)$$

The first equation is essentially Coulomb's law, and the latter is the Biot-Savart law for a system of moving charges.

To take into account accurately the retardation effects, the phase-space information of all nucleons before the moment t is required to calculate the electromagnetic fields at that moment. Some special care is thus necessary in initializing the reaction. In principle, the two colliding nuclei should be initialized to come from infinitely far away toward each other on their Coulomb trajectories. In practice, considering the need of keeping the initial nuclei stable and the computing time minimal, the initial distance between the surfaces of the two colliding nuclei is taken as 3 fm in our calculations. We make a precollision phase-space history for all nucleons assuming that they are frozen in the projectile or target moving with a center-of-mass velocity $\boldsymbol{v}_{p/t}$ (i.e., $\boldsymbol{r}_i=\boldsymbol{r}_i^0+\boldsymbol{v}_{p/t}t$, where $\boldsymbol{r}_i^0$ is the initial coordinate of the nucleon). As we show, comparisons of our transport-model calculations with analytical estimates for two moving charges (target and projectile) in both relativistic and nonrelativistic cases indicate that our method of handling the precollision phase-space histories of all nucleons is reasonable.

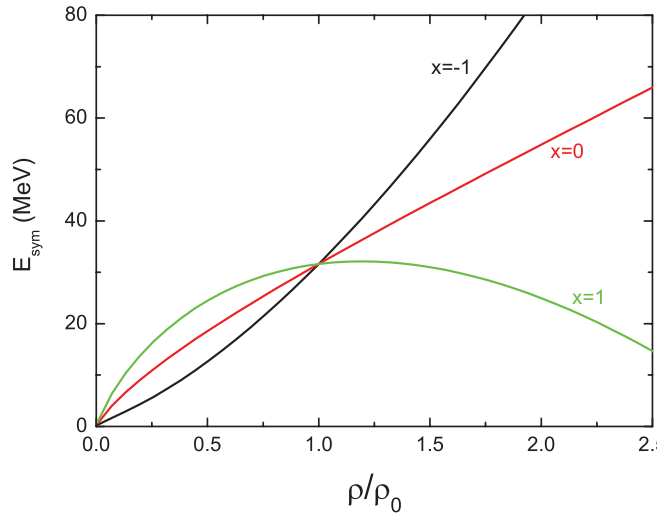

FIG. 1. (Color online) Density dependence of nuclear symmetry energy used in the IBUU11 calculations.

We refer to the BUU code used in this study, IBUU11. Compared to the IBUU04 code [20], where the momentum-dependent interaction (MDI) is used [22], in addition to the electromagnetic fields with retardation effects, an isospin-dependent three-body force [23] (instead of the standard one used in the MDI, Gogny and Skyrme effective interactions) is used. Moreover, the high-momentum tail of the MDI isoscalar potential is readjusted to better fit the nucleon optical potential from nucleon-nucleus scattering experiments. Details of these modifications and their effects on experimental observables are presented in a forthcoming publication [21]. In this work, we focus on the magnetic aspect of HICs at intermediate energies. Because one of our main motivations here is to see whether experimental observables known to be sensitive to $E_{\rm sym}(\rho)$ are affected by the magnetic effects, we notice here that in the IBUU11 model $E_{\rm sym}(\rho)$ is controlled by a parameter x introduced in the three-body part of the MDI [22,23]. By adjusting the parameter x, one can mimic diverse behaviors of the $E_{\rm sym}(\rho)$ predicted by various microscopic many-body theories [24]. As an example, shown in Fig. 1 are $E_{\rm sym}(\rho)$ with $x=1$, 0, and -1, respectively.

III. RESULTS AND DISCUSSIONS

In this section, we first illustrate and discuss the beam energy and impact parameter dependence of the time evolution and space distribution of the magnetic field. To help understand the magnetic effect in HICs, we also compare the Lorentz force with the Coulomb and nuclear forces. We then present and discuss magnetic effects on experimental observables.

A. Characteristics of internal electromagnetic fields in heavy-ion reactions

Features of the internal electromagnetic fields are independent of the symmetry energy parameter x. In this section,

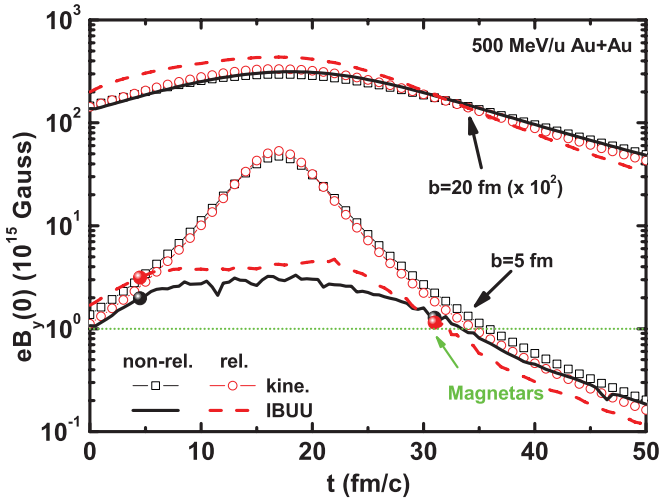

FIG. 2. (Color online) Time evolutions of the magnetic field strength $eB_y(0)$ at the center of mass of the reaction system for 500 MeV/nucleon (MeV/u) Au + Au reactions at $b = 5$ and 20 fm, respectively. The magnitude of $eB_y(0)$ for $b = 20$ fm is multiplied by 10^2 for clarity. The approximate beginning and ending of the overlap phase between the projectile and target are indicated by the small spheres (for $b = 20$ fm there is no overlap).

unless otherwise specified, a value of $x = \frac{1}{3}$ is used. We take the z (x) axis as the beam (impact parameter) direction. Based on the formula of magnetic field strength in Eq. (3), the dominant component of the internal magnetic field is in the y axis perpendicular to the reaction plane (z-x). The component in the reaction plane is negligible because of the slow motions of nucleons in the x or y directions, especially in the early phase of the reaction. To test our approach used in calculating the electromagnetic fields, we first compare the magnetic field $B_y(0)$ at the center of mass of the reaction system calculated using the full IBUU11 model dynamically with those measurements obtained under some limiting conditions for idealized situations. Shown in Fig. 2 are the values of $B_y(0)$ for Au + Au reactions at a beam energy of 500 MeV/nucleon and an impact parameter of $b = 5$ and 20 fm, respectively. As a reference, the approximate magnetic field on the surfaces of magnetars is also indicated. The legend "non-rel." and "rel." indicate the results obtained using Eqs. (5) and (3), respectively. For a comparison, we also performed calculations using both Eqs. (5) and (3) assuming that the projectile and target are two point charges located at their individual centers of mass and are moving with their initial velocities only. Results of this calculation are denoted by "kine." in Fig. 2. Several interesting observations can be made. First, it is seen that the values of $B_y(0)$ calculated with the nonrelativistic and relativistic formulas are very close to each other, for both kinematic and dynamical calculations, as one expects for reactions at relatively low beam energies. Second, the dynamical IBUU11 results and the kinematic estimates are very close at the beginning and the end of the reaction, but they are very different during the reaction phase spanned by the small spheres of the same color. The magnetic field has contributions from the projectilelike and targetlike spectators as well as charged particles in the participant region. Contributions from the latter, however, are very weak because of the approximately isotropic nucleon momentum distribution there. Once the projectile and target begin to overlap, nucleon-nucleon collisions start transferring the participants' longitudinal momenta into transverse directions. Thus, $B_y(0)$ from the IBUU11 model is weaker than the kinematic estimate during the reaction phase. We notice that the magnetic fields in the x and z directions are rather weak because they only come from charged participants which are moving essentially randomly in all possible directions. For the very peripheral reactions with $b = 20$ fm, the two nuclei do not overlap. Thus, as one expects, there is almost no difference between the kinematic and dynamical results. The aforementioned comparisons enhance our confidence in using the IBUU11 model to study the internal electromagnetic fields and their effects in HICs. In the following, we only present results calculated with the relativistic formula and the dynamical IBUU11 model.

The contours of the nucleon density ρ/ρ_0, the magnetic field strength eB_y, and the electric field strength eE_x in the x-z plane at $t = 10$, 20, 30, and 40 fm/c for the 500 MeV/nucleon Au + Au collisions at an impact parameter of $b = 10$ fm are shown in Fig. 3. We notice that both eB_y and eB_x are plotted in units of MeV^2, which is equal to 1.44×10^{13} G. For discussing the spatial distribution of the electromagnetic fields, we can divide the space into three zones in terms of the x coordinate: the outside zone, where $|x| > 15$ fm; the spectator zone, where $5 \leqslant |x| \leqslant 15$ fm; and the overlap zone, where $|x| < 5$ fm. As mentioned earlier, the electromagnetic fields come from both the spectators and the participants. In the outside zone, the spectator near the field point generates a stronger magnetic field in the negative y direction while the other spectator farther away generates a weaker magnetic field in the positive y direction. The superposition leads to a magnetic field that points to the negative y direction. However, the electric field eE_x in the outside zone includes contributions from all charges. Its sign is the same as the sign of the x coordinate of the field point. In the overlap zone, the magnetic fields generated by the two spectators superimpose constructively because they are all in the positive y direction, while the magnetic fields generated there by the moving charges in the participant region largely cancel each other. The strength of the magnetic field peaks when the two nuclei have reached the maximum compression. It then drops when the spectators depart from each other. The signs of the electric field in the x direction generated by the two spectators are always opposite, leading to the very weak electrical field in the participant region where the magnetic field is the strongest.

Next, we explore the impact-parameter and beam-energy dependence of the magnetic field at the center of mass of the reaction system. Shown in Fig. 4 is the impact-parameter dependence of $eB_y(0)$. The strength of the magnetic field grows with increasing impact parameter b up to about $b = 12$ fm. It then starts decreasing with larger b. This is easily understandable. There are basically two factors determining the magnetic field strength for a given beam energy. One is the position vector $\boldsymbol{R}$ from the moving charges to the field point, and the other is the charge number of the spectator, N_s. Their competition determines the strength of the magnetic field. As

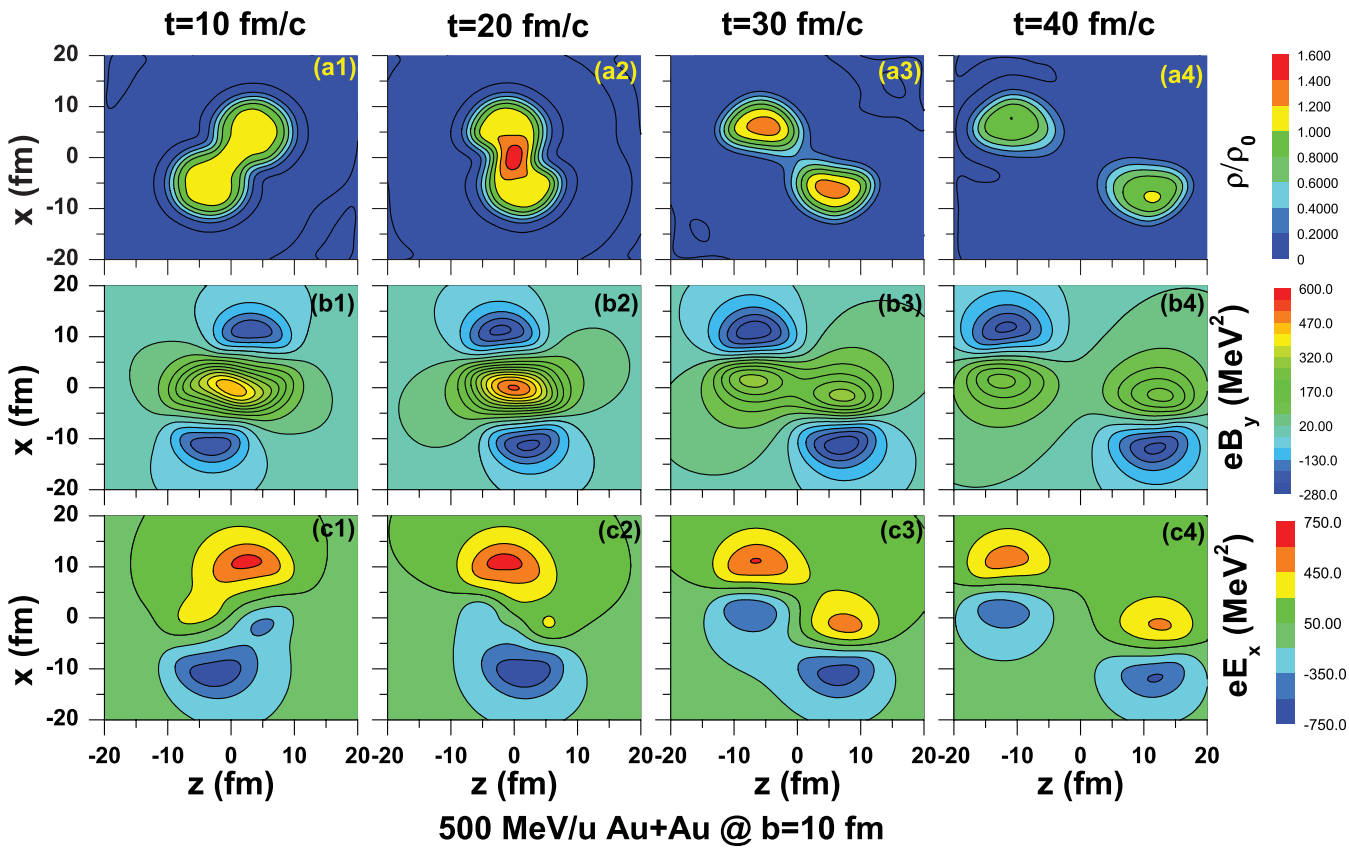

FIG. 3. (Color online) Distributions of the nucleon density ρ/ρ_0 (top), the magnetic field strength eB_y (middle), and the electrical field strength eE_x (bottom) in the x-z plane at $t = 10$, 20, 30, and 40 fm/c for the 500 MeV/nucleon Au + Au collisions at an impact parameter of $b = 10$ fm.

the impact parameter increases, while the spectators are farther away from the center they carry more charges. The net result is that the magnetic field becomes stronger with increasing impact parameter. However, as the impact parameter becomes larger than the sum of the radius of the projectile and target (e.g., when $b > 12$ fm for the Au + Au reaction), almost all charges are with the spectators, and the magnetic field is thus only determined by $\boldsymbol{R}$. Therefore, the reactions with larger impact parameters create weaker magnetic fields at the center of the reaction. Based on the IBUU11 results, off-central collisions with $b = 8 \sim 10$ fm seem to be the most suitable impact-parameter range to produce the strongest magnetic effect. These reactions create strong magnetic fields and there are also enough light charged particles moving in the magnetic fields to be detected in experiments.

For head-on collisions, equivalently there are two counter-currents approaching each other, leading to an approximately zero magnetic field at the center of the reaction. It is worth noting that the magnetic field at the center is not exactly zero but fluctuates within a small range. This is because the phase-space distribution of charges in the collision is not completely isotropic due to the finite number of test particles used. Moreover, because of the finite duration of the reaction, there are finite magnetic fields around both the projectile and the target as they approach each other. To be more quantitative, shown in Fig. 5 are the distributions of the magnetic field eB_y in the x-z plane at $t = 10$, 20, 30, and 40 fm/c for the head-on collision of Au + Au at a beam energy of 500 MeV/nucleon. In the early stage of the reaction when the projectile and target squeeze into each other, they create strong magnetic fields around them. Although the magnetic field at the center of the reaction is almost zero constantly, the magnetic fields at other locations vanish only in the late phase of the reaction, when an approximately isotropic momentum distribution indicating significant stopping is achieved. As we show later, the finite magnetic fields in the early stage of head-on collisions can influence the ratio of charged pions that are mostly created in the compression phase of the reaction.

Another factor determining the strength of the magnetic field is the velocity of spectators (i.e., the beam energy of the reaction). Shown in Fig. 6 is the beam-energy dependence of $eB_y(0)$. As one expects, although the maximum strength of the magnetic field increases with beam energy, the duration of the strong magnetic field decreases because the spectators leave the collision region quickly at higher beam energies. Compared to reactions at RHIC, the strength of the magnetic field is about 10 times lower but the reaction lasts about 10 times longer. Because observable effects of any force depend on not only its strength but also its duration, magnetic effects in HICs at intermediate energies are thus worth an investigation.

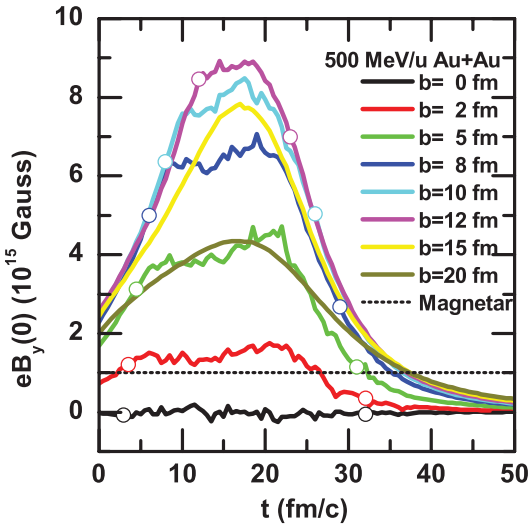

FIG. 4. (Color online) Impact-parameter dependence of $eB_y(0)$ for the 500 MeV/nucleon Au + Au collisions. Durations of the overlap between the projectile and the target are indicated roughly by the open circles (for $b = 15$, 20 fm there is no overlap). The thin black dotted line indicates the magnetic field strength at the surfaces of magnetars.

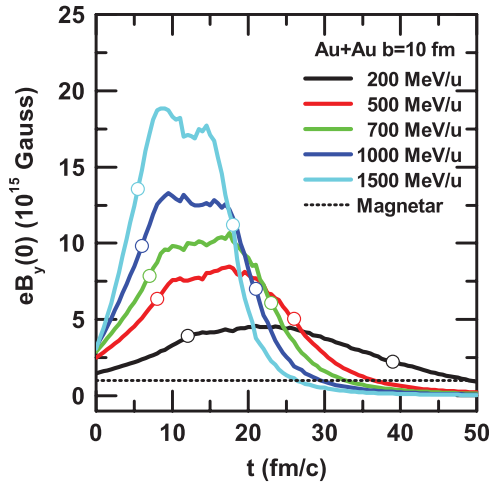

FIG. 6. (Color online) Beam-energy dependence of $eB_y(0)$ for the Au + Au collisions with $b = 10$ fm. Durations of the overlap between the projectile and target are indicated roughly by the open circles. The thin black dotted line indicates the magnetic field strength at the surfaces of magnetars.

B. Magnetic effects on observables in heavy-ion collisions

While no chiral magnetic effect is expected in HICs at intermediate energies, it is still interesting to examine magnetic effects on hadronic observables. First of all, we would like to mention that the effects of strong magnetic fields on the equation of state (EOS) of cold hadronic and quark matter including the Landau quantization and the nucleon anomalous magnetic moment in neutron stars have been studied extensively (see, e.g., Refs. [25–29]). It has been shown consistently that the magnetic effects become significant only for magnetic fields stronger than about 1×10^{18} G. Moreover, at finite temperature some of the magnetic effects get mostly washed out [29]. Because the temperature is high and the

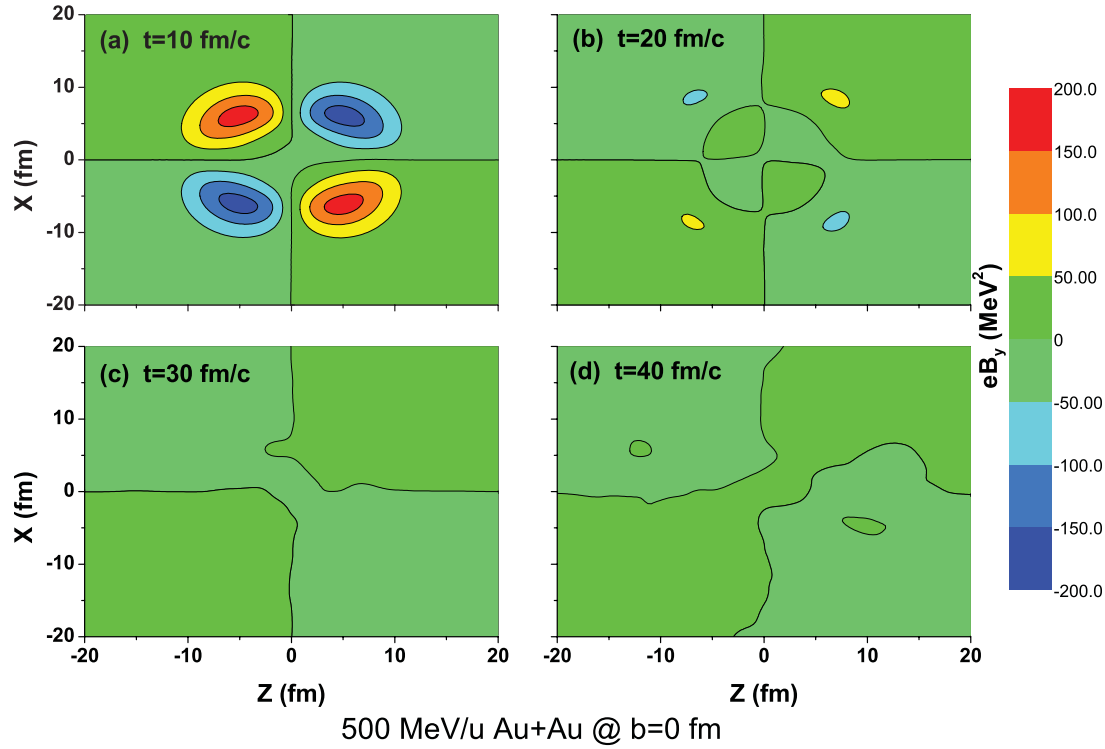

FIG. 5. (Color online) Distributions of the magnetic field strength eB_y in the x-z plane at $t = 10$, 20, 30, and 40 fm/c for the head-on collisions of Au + Au at a beam energy of 500 MeV/nucleon.

maximum strength of the magnetic field created is still below 1×10^{18} G even at RHIC energies, it is not necessary to consider the effects of the magnetic field on the nuclear EOS. Instead, we focus directly on magnetic effects caused by the Lorentz force acting on moving charges. In the following, we examine separately magnetic effects on nucleons and pions.

1. Lorentz force compared with the Coulomb and nuclear forces

For nucleons, the magnetic effects are expected to be negligible because the Lorentz force is known to be very small compared to the nuclear force. However, while the electrical and magnetic fields are strongly correlated, the Coulomb force has been routinely taken into account but the Lorentz force is normally neglected in modeling HICs. To check the validity of this practice and obtain a more quantitative understanding about the relative importance of the Lorentz, Coulomb, and nuclear forces, we examine in Fig. 7 the ratios of the Lorentz force over the Coulomb and nuclear forces for a test charge. For this illustration only 500 test particles are used. To be specific, we calculate the ratio $R_x^{\rm ME}$ of the x component of the Lorentz force over that of the Coulomb force for a test charge in the outside zone. As a reference, we first make an analytical analysis for a simplified case. For a test charge located at the surface of the projectile moving on the trajectory of $\boldsymbol{r}(-\frac{b}{2} - R, 0, z_0 + v_0 t)$, where R, z_0, and v_0 are the radii, initial z coordinate, and the beam velocity, respectively, assuming the electromagnetic fields are due to two moving point charges (projectile and target) given by Eqs. (4) and (5), $R_x^{\rm ME}$ is simply

$$R_x^{\rm ME} = \frac{F_x^{\rm M}}{F_x^{\rm E}} = \frac{e v_z B_y}{e E_x} = \left(\frac{v_0}{c}\right)^2. \tag{6}$$

Thus, it is clear that, only for fast-moving particles likely existing in reactions at high beam energies, the Lorentz force is expected to be significant compared to the Coulomb force. We now examine numerically $R_x^{\rm ME}$ for the test charge using the electromagnetic fields calculated with the IBUU11 model. In Fig. 7(a), the time evolution of $R_x^{\rm ME}$ is shown for several impact parameters for the 500 MeV/nucleon Au + Au reactions. The evolution can be approximately divided into four periods. Before the two nuclei get in touch, $R_x^{\rm ME} = 0.21$, which is exactly the same as the prediction of Eq. (6). In

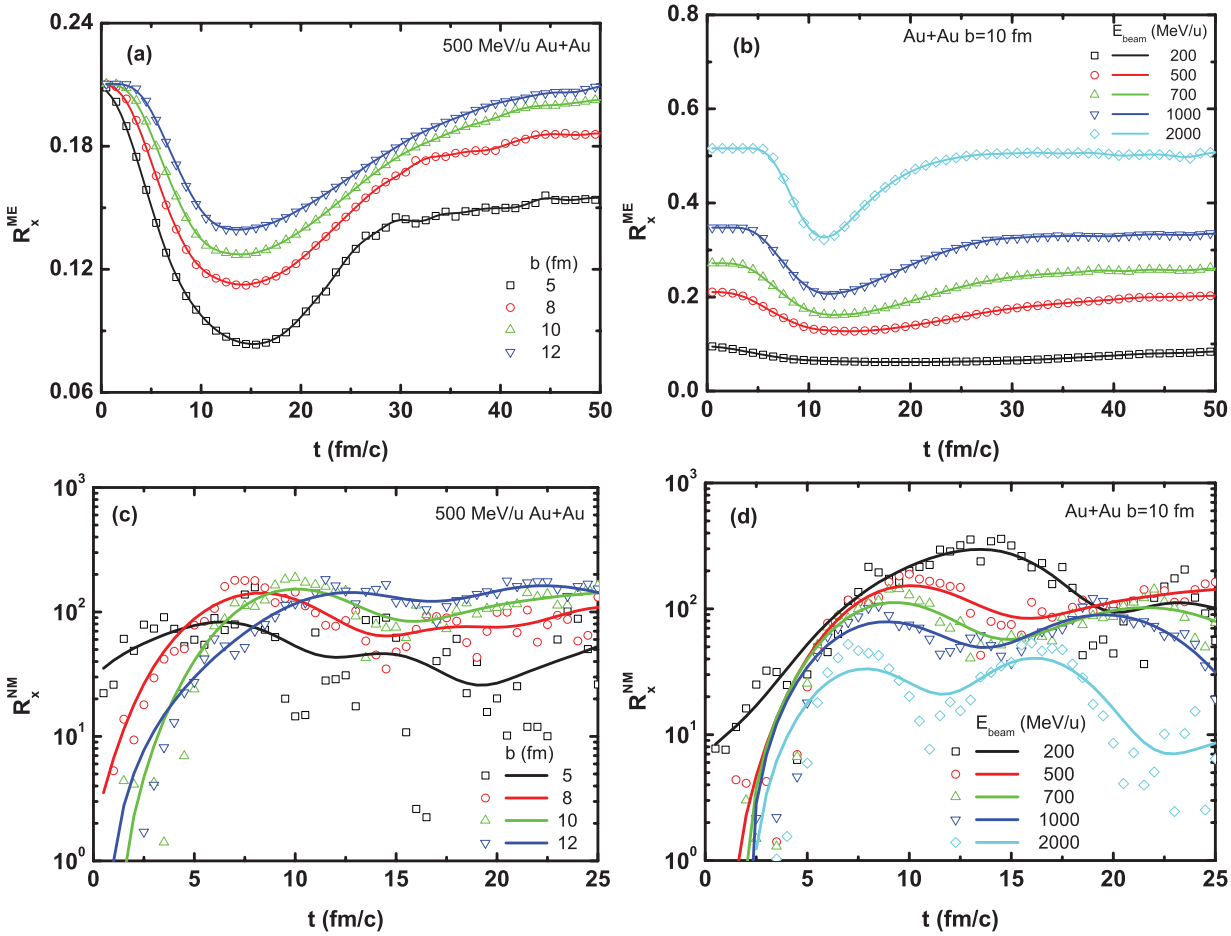

FIG. 7. (Color online) The ratio between the x components of the magnetic and electric forces ($R_x^{\rm ME}$) (a) at various impact parameters for the 500 MeV/nucleon Au + Au reactions and (b) at various incident energies for the Au + Au reactions with $b = 10$ fm; and the ratio between the x components of the magnetic and nuclear forces ($R_x^{\rm NM}$) (c) at various impact parameters for the 500 MeV/nucleon Au + Au reactions and (d) at various incident energies for the Au + Au reactions with $b = 10$ fm (the lines are the results smoothed with the fast Fourier transform filter to guide the eye).

the compression phase, because the magnetic fields in the outside region generated by the projectilelike and targetlike spectators are in the opposite directions, the net magnetic field decreases, whereas the electric field there becomes stronger. Consequently, $R_x^{\rm ME}$ drops until about 15 fm/c. In the expansion phase, the situation is reversed. After the collisions are over, the $R_x^{\rm ME}$ keeps an approximately constant value smaller than $(v_0/c)^2$ depending on the impact parameter. The beam-energy dependence shown in Fig. 7(b) for the Au + Au reactions with $b = 10$ fm can be similarly understood. We notice that $R_x^{\rm ME} = (v_0/c)^2$ at the beginning of the collision is satisfied at all beam energies. As the incident energy increases, the Lorentz force becomes closer to the Coulomb force.

We now turn to the ratio between the x components of the nuclear and Lorentz forces (i.e., $R_x^{\rm NM} = F_x^{\rm N}/F_x^{\rm M}$) for a test proton at the center of mass with a constant velocity of $v_z = v_0$. Shown in Figs. 7(c) and 7(d) are the impact-parameter and beam-energy dependences of $R_x^{\rm NM}$. Because the nuclear force is proportional to the gradient of the single-nucleon potential (i.e., $F^{\rm M} = -\nabla_r U$), large fluctuations are seen in $R_x^{\rm NM}$. It is seen that the nuclear force is several tens to 10^2 times larger than the Lorentz force. The magnetic field is thus not expected to affect the reaction dynamics and nucleon observables. Therefore, it is not surprising that nuclear reaction models can describe most experimental data without considering any magnetic effect at all.

2. *Magnetic effects on collective observables of nucleons and pions*

Although the magnetic effects on nucleon observables are expected to be very small, to be quantitative, it is still necessary to examine how small the effects are. From the expression of the Lorentz force $F^{\rm M} = q\boldsymbol{v} \times \boldsymbol{B}$, it is easy to see that the main component of the Lorentz force is in the reaction plane (especially in the x direction). The average transverse momentum in the reaction plane (i.e., $\langle p_x \rangle$) is thus a quantity most likely to be affected. Shown in the top panels of Fig. 8 are the average in-plane transverse momentum as a function of rapidity and the so-called in-plane transverse flow [30] for free protons and pions, respectively. Indeed, there is essentially no magnetic effect on nucleons. It is seen that both negative and positive pions flow in the same direction as nucleons but with much lower transverse momentum in the reaction plane [31]. Interestingly, there is a very weak indication of some magnetic effects on the $\langle p_x(y) \rangle$ of pions at forward

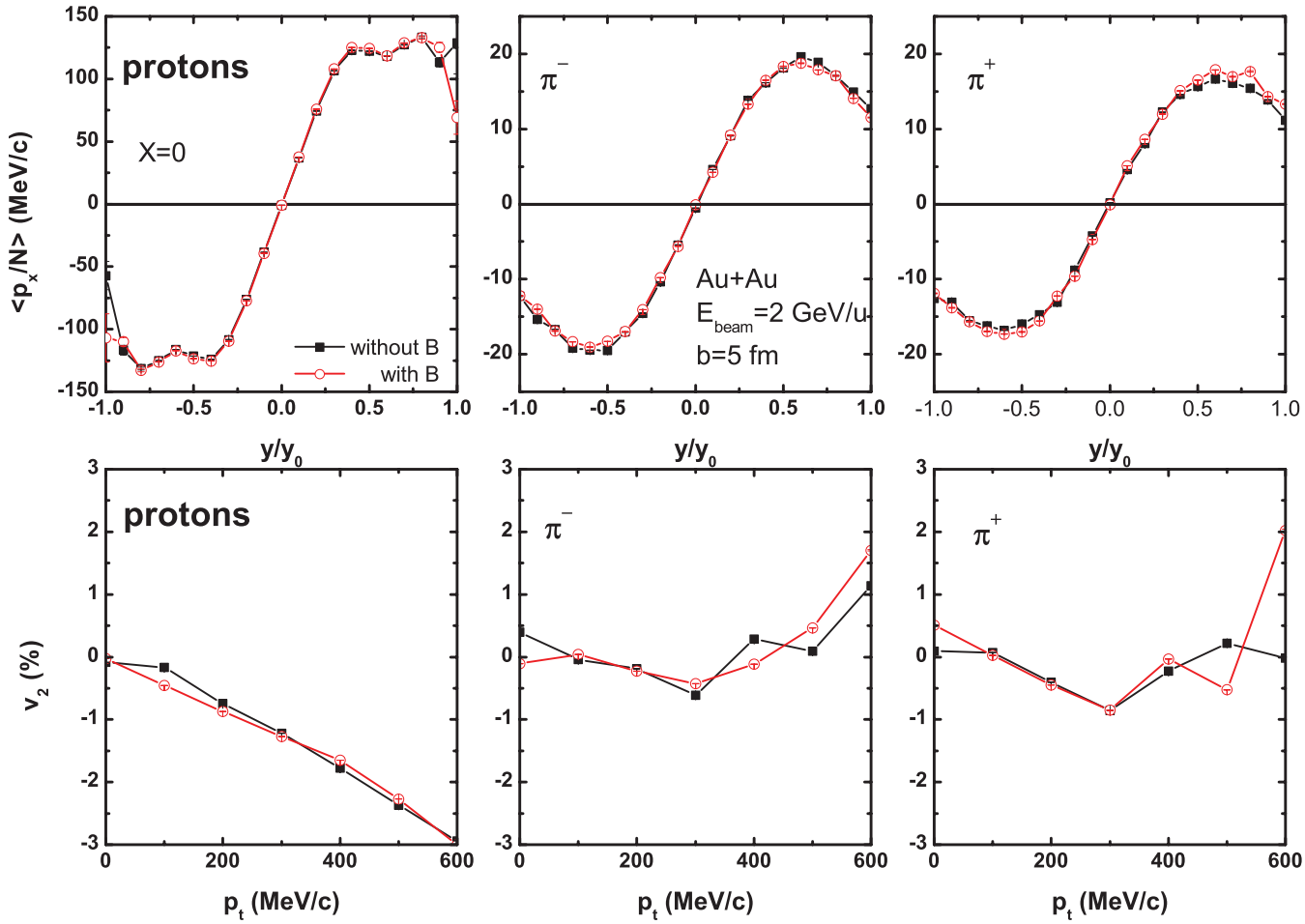

FIG. 8. (Color online) (top) The average in-plane transverse momentum of free protons and pions as a function of rapidity. (bottom) Elliptic flow for free protons and pions as a function of transverse momentum for the 2 GeV/nucleon Au + Au reaction at an impact parameter of 5 fm with $x = 0$.

and backward rapidities. This is qualitatively understandable. The Lorentz force influences pions more easily because they are light compared to nucleons. Moreover, it also indicates that the magnetic field decreases (increases) very slightly the magnitude of $\langle p_x \rangle$ for positive (negative) pions at both forward and backward rapidities due to the magnetic focusing and defocusing effects, which we discuss in detail in the next section. Next, we investigate in the lower panels of Fig. 8 the so-called differential elliptic flow as a function of transverse momentum [32,33],

$$\langle v_2(p_t) \rangle = \frac{1}{N} \sum_{i=1}^{N} \frac{p_{ix}^2 - p_{iy}^2}{p_{ix}^2 + p_{iy}^2}, \tag{7}$$

where N is the total number of free particles. The p_{iy} is the ith particle's transverse momentum perpendicular to the reaction plane. Again, there is essentially no magnetic effect on the differential elliptical flow of both nucleons and pions.

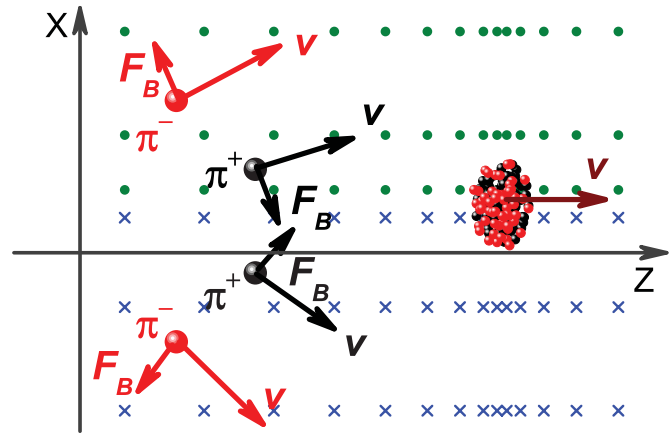

FIG. 9. (Color online) A sketch illustrating the Lorentz forces on charged pions in the magnetic field created by the projectilelike spectator. Positive pions are focused into smaller polar angles while negative pions are defocused into larger polar angles regardless of whether they are moving above or below the spectator.

3. *Magnetic effects on the π^-/π^+ and neutron-to-proton ratios*

It is well known that the Coulomb force affects significantly the π^-/π^+ ratio in HICs. The so-called Coulomb peak often appears near the projectile and/or target rapidities. This phenomenon has been studied extensively both experimentally [34–38] and theoretically [39–44] since the 1970s (see, e.g., Ref. [45] for a review). However, to our best knowledge, magnetic effects were not considered in any of these studies. Although the Lorentz force on pions is normally smaller than the Coulomb force, they have the same order of magnitude. Moreover, compared to nucleons, pions are light with relatively higher speeds and are thus more easily affected by the Lorentz force. Furthermore, there is no nuclear force acting on pions once they are produced, at least in most model simulations where pions change their momenta only through pion-hadron collisions and the Coulomb field. To our best knowledge, theoretical studies on the mean field (dispersion relation) for pions are still rather inconclusive [46]. Thus, most transport models neglect the mean field for pions. Considering all of the above, the magnetic force on pions can be significant. In fact, we expect the Lorentz and Coulomb forces to have opposite effects on the π^-/π^+ ratio. Namely, near the projectile or target rapidity the Coulomb force increases the π^-/π^+ ratio whereas the Lorentz force reduces it. Effects of the Lorentz forces on positive and negative pions are illustrated in Fig. 9 using the projectilelike spectator as an example. The moving track of the spectator can be regarded as a current. Above (below) the current, the magnetic field is perpendicular to the reaction plane and points outward (inward). The Lorentz force focuses the π^+ into smaller forward (backward) polar angles while it defocuses the π^- to larger forward (backward) polar angles. So the π^-/π^+ ratios at large rapidities are reduced by the Lorentz force. Moreover, owing to the magnetic focusing and defocusing effect on positive and negative charges, the changes in transverse momentum for particles above and below the current are opposite. So the total magnetic effect on the average transverse momentum in the reaction plane is very tiny even for pions. This explains why the magnetic effects on the transverse flow $\langle p_x(y) \rangle$ and the differential elliptical flow $v_2(p_t)$ are negligible for both nucleons and pions.

Why is it so important to understand clearly and precisely the electromagnetic effects on the π^-/π^+ ratio? One special reason is that the π^-/π^+ ratio was predicted as one of the most promising probes of the nuclear symmetry energy at suprasaturation densities [47]. Although comparisons of transport model predictions [48–50] with existing data [51] are still inconclusive, all models have consistently shown that the π^-/π^+ ratio is rather sensitive to the high-density behavior of the nuclear symmetry energy. The latter is rather poorly known, as indicated in Fig. 1. In fact, even the trend of the symmetry energy at suprasaturation densities, namely, whether it increases or decreases with increasing density, is still controversial partially because of our poor knowledge about the isospin dependence of strong interaction. To extract reliably accurate information from the π^-/π^+ ratio about the high-density behavior of nuclear symmetry energy, it is thus necessary to understand precisely the effects from the well-known electromagnetic interactions. So, how strong is the magnetic effect on the π^-/π^+ ratio in comparison to the symmetry-energy effect? To answer this question and give a quantitative example, we show in Fig. 10 the π^-/π^+ ratio as a function of rapidity with and without the magnetic field calculated with three different values of the symmetry energy parameter x for the 2 GeV/nucleon Au + Au reactions at an impact parameter of $b = 0$ and 5 fm, respectively. In each case considered here, 200 000 IBUU11 events are used. Comparing the results obtained with and without the magnetic field using any of the x parameters considered, it is seen that magnetic effects on the π^-/π^+ ratio are significant compared to the symmetry-energy effect, especially at forward and backward rapidities and particularly for midcentral collisions. Quantitatively, the π^-/π^+ ratio obtained with the magnetic field is significantly lower at forward and backward rapidities (polar angles) due to the magnetic focusing and defocusing effects on the positive and negative pions, as we

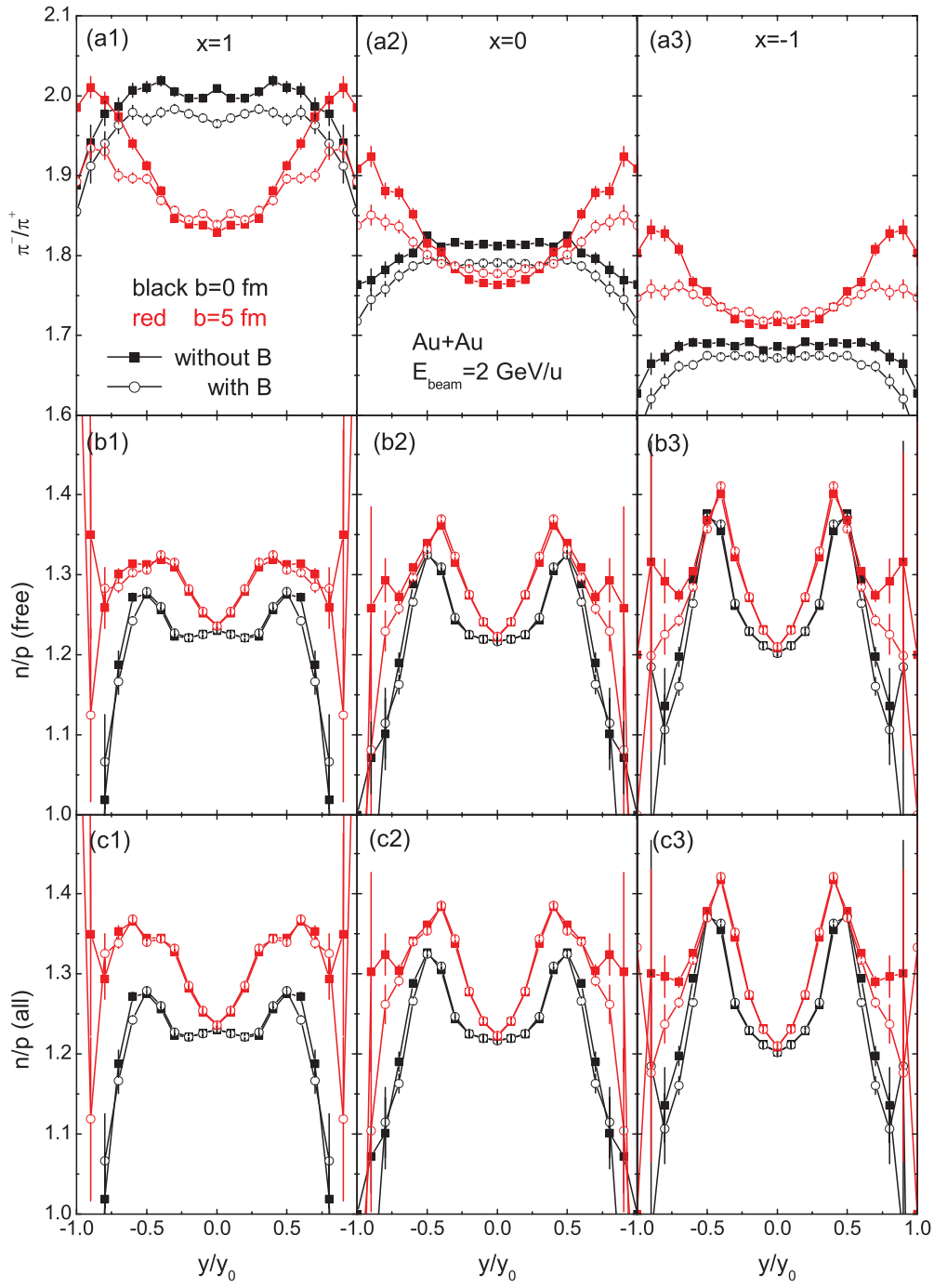

FIG. 10. (Color online) The π^-/π^+ ratio (top), the neutron-to-proton ratio, n/p, of free (middle) and all (bottom) nucleons as a function of rapidity with and without the magnetic field, calculated with the three different values of symmetry- energy parameter x for the reactions of 2 GeV/nucleon Au + Au at impact parameters $b = 0$ and 5 fm, respectively.

illustrated in Fig. 9. Pions at higher rapidities have larger longitudinal momenta and thus feel stronger Lorentz forces compared to those at midrapidity. For the head-on collisions, the magnetic effect on the π^-/π^+ ratio is small but still appreciable. This observation requires some explanations. As shown earlier in Fig. 5, in the compression phase of the reaction when most pions are produced, even in head-on collisions there are considerable magnetic fields around both projectile and target spectators, although the magnetic field is approximately zero at the center of the reaction. Thus, it is understandable that the π^-/π^+ ratio in head-on collisions is also affected by the magnetic field. From peripheral to head-on collisions, the π^-/π^+ ratio changes gradually from forward-backward peaked to center-peaked distributions. In peripheral collisions, there are significant Coulomb effects due to the spectators. One thus expects the π^-/π^+ ratio to peak at forward-backward

rapidities. It is seen that the magnetic effect at forward-backward rapidities is compatible with the symmetry-energy effect from changing the x parameter by one unit. Thus, compared to the symmetry-energy effect, the magnetic effect on the π^-/π^+ ratio is significant. Overall, the π^-/π^+ ratio decreases as the symmetry energy at suprasaturation densities becomes stiffer when the parameter x changes from 1 to -1. For comparisons, the neutron-to-proton ratio n/p of free (selected as those with local density less than $\rho_0/8$ at freeze-out) and all nucleons are shown as functions of rapidity in the middle and bottom panels of Fig. 10, respectively. It is seen that there is essentially no noticeable magnetic effects within error bars on the n/p ratios. This is consistent with our expectation and the results on the transverse and elliptical flows discussed earlier. The nonuniform n/p and π^-/π^+ ratios as functions of rapidity indicate the lack of complete isospin equilibrium for both nucleon and pion components. This is the so-called isospin translucency expected in heavy-ion reactions at the beam energies studied here [52,53].

It is worth noticing that so far only the integrated π^-/π^+ ratio (i.e., the ratio of total π^- to π^+ multiplicities) has been used in attempts to constrain the symmetry energy at high densities without considering the magnetic effects. Whereas the integrated π^-/π^+ ratio is rather sensitive to the symmetry-energy parameter x in reactions near the pion production threshold, as the beam energy becomes higher than about 1 GeV/nucleon, the sensitivity gradually disappears [48]. It is thus interesting to see that the rapidity distribution of the $\pi^-/\pi^+(y)$ ratio shows a strong sensitivity to the parameter x even in the reactions at a beam energy of 2 GeV/nucleon, where the baryon density can reach about $3.5\rho_0$. Thus, the differential $\pi^-/\pi^+(y)$ ratio is a potentially useful probe of the high-density behavior of the nuclear symmetry energy. Nevertheless, because the strongest sensitivity to the symmetry energy is at forward and backward rapidities, where the π^-/π^+ ratio is also strongly affected by the magnetic field, special care must be taken in both model calculations and the data analysis. We notice that most of the currently available detectors, including the one used by the FOPI Collaboration [51], do not provide full coverage at very forward and/or backward angles. The integrated π^-/π^+ ratio is normally obtained by extrapolating the angular distributions of pions measured in a limited angular range to all polar angles. Although this procedure ignores the magnetic effects on the angular distribution of pions, the effects of the magnetic field on the integrated π^-/π^+ ratio is small. Shown in Table I are the integrated π^-/π^+ and neutron-to-proton ratios calculated without and with the magnetic field. It is seen that the integrated ratios are not affected much by the magnetic field. This is what we expected because the Lorentz force affects differently only the angular distributions of positively and negatively charged particles, not their total multiplicities. Also, consistent with previous findings [48], the integrated π^-/π^+ ratio at beam energies higher than about 1 GeV/nucleon is not so sensitive to the variation of the symmetry energy, whereas there is a clear indication that a higher π^-/π^+ ratio is obtained with a softer $E_{\rm sym}(\rho)$ at suprasaturation densities. Thus, the differential $\pi^-/\pi^+(y)$ ratio is a better probe of the symmetry energy at suprasaturation densities after taking care of the magnetic effects using detectors covering very forward and/or backward polar angles.

TABLE I. Integrated π^-/π^+ and n/p ratios calculated without/with the magnetic field using three values of the symmetry-energy parameter $x = 1$, 0, and -1.

Ratio	b (fm)	$x = 1$	$x = 0$	$x = -1$
π^-/π^+	0	2.02/1.97	1.81/1.78	1.68/1.67
	5	1.87/1.86	1.79/1.79	1.73/1.73
n/p (free)	0	1.23/1.23	1.24/1.24	1.25/1.25
	5	1.28/1.28	1.29/1.29	1.29/1.29
n/p (all)	0	1.23/1.23	1.24/1.24	1.25/1.25
	5	1.31/1.31	1.31/1.31	1.32/1.32

IV. SUMMARY

In summary, within the transport model IBUU11, the time evolution and space distribution of internal electromagnetic fields in HICs at beam energies between 200 and 2000 MeV/nucleon are studied. Although the magnetic field can reach about 7×10^{16} G, it has almost no effect on nucleon observables because the Lorentz force is normally much weaker than the nuclear force. However, the magnetic field has a strong focusing and defocusing effect on positive and negative pions at forward and/or backward rapidities. Consequently, the differential $\pi^-/\pi^+(y)$ ratio as a function of rapidity y, but not the integrated one, is significantly altered by the magnetic field. At beam energies above about 1 GeV/nucleon, the differential $\pi^-/\pi^+(y)$ ratio is more sensitive to $E_{\rm sym}(\rho)$ than the integrated π^-/π^+ ratio. Our findings suggest that magnetic effects should be carefully considered in future studies of using the differential π^-/π^+ ratio as a probe of $E_{\rm sym}(\rho)$ at suprasaturation densities.

ACKNOWLEDGMENTS

We would like to thank Dr. N. Chamel, Dr. W. G. Newton, and Dr. C. Providencia for helpful discussions and information on magnetic effects in neutron stars, and Dr. Lie-Wen Chen and Dr. Chang Xu for collaborations in developing the IBUU11 code used in this study. We would also like to thank Dr. Derek Harter, who made our very intensive calculations possible within a rather short time by providing us access to the high-performance Computational Science Research Cluster at Texas A&M University, Commerce. This work was supported in part by the NSF under Grants No. PHY-0757839 and No. PHY-1068022, by NASA under Grant No. NNX11AC41G issued through the Science Mission Directorate, and by the National Natural Science Foundation of China under Grants No. 11005022, No. 10847004, and No. 11075215.

[1] Y. Sofue, M. Fujimoto, and R. Wielebinski, Annu. Rev. Astron. Astrophys. **24**, 459 (1986).
[2] K. Kawabata, M. Fujimoto, Y. Sofue, and M. Fukui, Publ. Astron. Soc. Jpn. **21**, 293 (1969).
[3] K. Dimopoulosa and A.-C. Davis, Phys. Lett. B **390**, 87 (1997).
[4] D. Grasso and H. R. Rubinstein, Phys. Rep. **348**, 163 (2001).
[5] C. Kouveliotou *et al.*, Nature (London) **393**, 235 (1998).
[6] A. I. Ibrahim, S. Safi-Harb, J. H. Swank, W. Parke, S. Zane, and R. Turolla, Astrophys. J. Lett. **574**, L51 (2002).
[7] M. A. Ruderman, L. Tao, and W. Kluzniak, Astrophys. J. **542**, 243 (2000).
[8] S. A. J. Wiegers, J. A. A. J. Perenboom, and J. C. Maan, J. Phys.: Conf. Ser. **51**, 595 (2006).
[9] [http://www.magnet.fsu.edu]
[10] J. Rafelski and B. Müller, Phys. Rev. Lett. **36**, 517 (1976).
[11] D. E. Kharzeev, L. D. McLerran, and H. J. Warringa, Nucl. Phys. A **803**, 227 (2008).
[12] V. Skokov, A. Illarionov, and V. Toneev, Int. J. Mod. Phys. A **24**, 5925 (2009).
[13] Dmitri E. Kharzeev and Ho-Ung Yee, Phys. Rev. D **83**, 085007 (2011), and references therein.
[14] D. Kharzeev, Phys. Lett. B **633**, 260 (2006).
[15] D. Kharzeev and A. Zhitnitky, Nucl. Phys. A **797**, 67 (2007).
[16] S. A. Voloshin, Phys. Rev. Lett. **105**, 172301 (2010).
[17] STAR Collaboration, B. I. Abelev *et al.*, Phys. Rev. Lett. **103**, 251601 (2009).
[18] STAR Collaboration, B. I. Abelev *et al.*, Phys. Rev. C **81**, 054908 (2010).
[19] V. Voronyuk, V. D. Toneev, W. Cassing, E. L. Bratkovskaya, V. P. Konchakovski, and S. A. Voloshin, Phys. Rev. C **83**, 054911 (2011).
[20] B. A. Li, C. B. Das, S. Das Gupta, and C. Gale, Phys. Rev. C **69**, 011603(R) (2004); Nucl. Phys. A **735**, 563 (2004).
[21] B. A. Li, L. W. Chen, L. Ou, and C. Xu (unpublished).
[22] C. B. Das, S. Das Gupta, C. Gale, and B. A. Li, Phys. Rev. C **67**, 034611 (2003).
[23] C. Xu and Bao-An Li, Phys. Rev. C **81**, 044603 (2010).
[24] Bao-An Li, Lie-Wen Chen, and Che Ming Ko, Phys. Rep. **464**, 113 (2008).
[25] A. Broderick, M. Prakash, and J. M. Lattimer, Astrophys. J. **537**, 351 (2000).
[26] C. Y. Cardall, M. Prakash, and J. M. Lattimer, Astrophys. J. **554**, 322 (2001).
[27] D. Bandyopadhyay, S. Chakrabarty, and S. Pal, Phys. Rev. Lett. **79**, 2176 (1997).
[28] A. Rabhi and C. Providencia, J. Phys. G: Nucl. Part. Phys. **35**, 125201 (2008).
[29] A. Rabhi, P. K. Panda, and C. Providencia, Phys. Rev. C **84**, 035803 (2011).
[30] P. Danielewicz and G. Odyniec, Phys. Lett. B **157**, 146 (1985).
[31] Bao-An Li, Nucl. Phys. A **570**, 797 (1994); Phys. Rev. C **50**, 2144 (1994).
[32] J.-Y. Ollitrault, Nucl. Phys. A **638**, 195c (1998).
[33] A. M. Poskanzer and S. A. Voloshin, Phys. Rev. C **58**, 1671 (1998).
[34] K. L. Wolf *et al.*, Phys. Rev. Lett. **42**, 1448 (1979).
[35] K. Nakai, J. Chiba, I. Tanihata, M. Sasao, H. Bowman, S. Nagamiya, and J. O. Rasmussen, Phys. Rev. C **20**, 2210 (1979).
[36] W. Benenson *et al.*, Phys. Rev. Lett. **43**, 683 (1979).
[37] H. M. A. Radi, J. O. Rasmussen, J. P. Sullivan, K. A. Frankel, and O. Hashimoto, Phys. Rev. C **25**, 1518 (1982).
[38] S. Schnetzer *et al.*, Phys. Rev. Lett. **49**, 989 (1982).
[39] K. G. Libbrecht and S. E. Koonin, Phys. Rev. Lett. **43**, 1581 (1979).
[40] G. F. Bertsch, Nature (London) **283**, 280 (1980).
[41] M. Gyulassy and S. K. Kauffmann, Nucl. Phys. A **362**, 503 (1981).
[42] A. Bonasera and G. F. Bertsch, Phys. Lett. B **195**, 521 (1987).
[43] B. Noren *et al.*, Nucl. Phys. A **489**, 763 (1988).
[44] B. A. Li, Phys. Rev. C **50**, 2144 (1994); Phys. Lett. B **346**, 5 (1995).
[45] R. Stock, Phys. Rep. **135**, 259 (1986).
[46] J. L. Nagle, P. Steinberg, and W. A. Zajc, Phys. Rev. C **81**, 024901 (2010).
[47] B. A. Li, Phys. Rev. Lett. **88**, 192701 (2002); Nucl. Phys. A **708**, 365 (2002).
[48] Z. G. Xiao, B. A. Li, L. W. Chen, G. C. Yong, and M. Zhang, Phys. Rev. Lett. **102**, 062502 (2009).
[49] Z. Q. Feng and G. M. Jin, Phys. Lett. B **683**, 140 (2010).
[50] V. Prassa, G. Ferini, T. Gaitanos, H. H. Wolter, G. A. Lalazissis, and M. Di Toro, Nucl. Phys. A **789**, 311 (2007).
[51] W. Reisdorf *et al.*, Nucl. Phys. A **781**, 459 (2007).
[52] B. A. Li and S. J. Yennello, Phys. Rev. C **52**, 1746(R) (1995).
[53] B. A. Li, C. M. Ko, and W. Bauer, Top. Rev.: Int. J. Mod. Phys. E **7**, 147 (1998).